Epitaxial $YBa_2Cu_3O_7$ on Biaxially Textured Nickel (001): An Approach to Superconducting Tapes with High Critical Current Density

David P. Norton, Amit Goyal, John D. Budai, David K. Christen, Donald M. Kroeger, Eliot D. Specht, Qing He, Bernd Saffian, M. Paranthaman, Charles E. Klabunde, Dominic F. Lee, Brian C. Sales, Fred A. List

In-plane–aligned, *c* axis–oriented $YBa_2Cu_3O_7$ (YBCO) films with superconducting critical current densities J_c as high as 700,000 amperes per square centimeter at 77 kelvin have been grown on thermomechanically rolled-textured nickel (001) tapes by pulsed-laser deposition. Epitaxial growth of oxide buffer layers directly on biaxially textured nickel, formed by recrystallization of cold-rolled pure nickel, made possible the growth of YBCO films 1.5 micrometers thick with superconducting properties that are comparable to those observed for epitaxial films on single-crystal oxide substrates. This result represents a viable approach for the production of long superconducting tapes for high-current, high-field applications at 77 kelvin.

Since the discovery of high-temperature superconductivity (HTS) in cuprate materials, substantial efforts have focused on developing a high-current superconducting wire technology for applications at 77 K (*1*, *2*). Early in these efforts it was observed that randomly oriented polycrystalline HTS materials have critical current densities, J_c, <500 A/cm^2. In contrast, oriented YBCO thin films grown epitaxially on single-crystal oxide substrates, such as $SrTiO_3$ (001), exhibit J_c values >1 MA/cm^2 at 77 K (*3*). This huge difference between randomly oriented HTS ceramics and single crystal–like epitaxial films is directly related to the misorientation angles at the grain boundaries in polycrystalline materials. Values for J_c across a grain boundary decrease significantly as the misorientation angle increases, with weak-link behavior observed for misorientation angles at the grain boundaries greater than ~10° (*4*–*12*). In order to achieve high J_c values (~10^5 to 10^6 A/cm^2, 77 K), the crystallographic orientation of the HTS superconducting wire or tape must have a high degree of both in-plane and out-of-plane grain alignment over the conductor's entire length. Ideally, this would be achieved with YBCO, because the limits for dissipation-free current at 77 K in an applied magnetic field are most favorable for this material (*13*, *14*).

D. P. Norton, J. D. Budai, D. K. Christen, Q. He, B. Saffian, C. E. Klabunde, B. C. Sales, Solid State Division, Oak Ridge National Laboratory (ORNL), Post Office Box 2008, Oak Ridge, TN 37831–6056, USA.
A. Goyal, D. M. Kroeger, E. D. Specht, D. F. Lee, F. A. List, Metals and Ceramics Division, ORNL, Post Office Box 2008, Oak Ridge, TN 37831–6116, USA.
M. Paranthaman, Chemical and Analytical Sciences Division, ORNL, Post Office Box 2008, Oak Ridge, TN 37831–6100, USA.

One approach to producing a high-J_c HTS tape is to deposit a thick epitaxial film on a substrate material that has a high degree of in-plane and out-of-plane crystallographic texture and can be produced in long lengths. Epitaxial HTS films on single-crystal oxides satisfy the requirements for high J_c, but it is not feasible to produce long lengths of these substrates. Recent efforts have focused on the use of ion beam–assisted deposition (IBAD) to achieve in-plane alignment of oxide buffer layers on polycrystalline metal substrates for subsequent epitaxial growth of YBCO (*15*–*19*). Indeed, a modest degree of in-plane texture for *c* axis–oriented YBCO films made by IBAD results in a significant increase in J_c, with values ranging from 10^5 to 10^6 A/cm^2 at 77 K. However, IBAD techniques have limitations, including the relatively low deposition rates associated with the IBAD buffer layers as well as difficulties in consistently producing in-plane crystallographic alignment of less than 10°, that may limit the use of this technique in commercial production.

We report here an alternative approach for achieving in-plane–aligned, high-J_c YBCO films on long substrates without IBAD. A biaxially textured Ni (001) tape, formed by recrystallization of cold-rolled pure Ni (*20*, *21*), is used as the initial, in-plane–aligned substrate. A (001)-oriented oxide buffer layer architecture is then epitaxially grown that maintains the sharp crystallographic cube texture of the metal substrate while providing a barrier to chemical interaction with the Ni. Subsequent growth of YBCO on this structure, referred to as a rolling-assisted, biaxially textured substrate (RABiTS), results in *c* axis–oriented, in-plane–aligned films with J_c values as high as 700,000 A/cm^2 at 77 K. The advantage of this approach over other alternatives, such as IBAD, is in the simplicity of producing the initial in-plane alignment, required for high J_c, by a cold-rolling and annealing process that can easily be scaled to produce arbitrary substrate lengths.

The YBCO/yttria-stabilized ZrO_2 (YSZ)/CeO_2 layered architecture used to grow in-plane–aligned, high-J_c films on rolled-textured Ni (001) is schematically illustrated in Fig. 1. The Ni substrates have a relatively sharp cubic orientation with a full width at half maximum (FWHM) out-of-plane texture $\Delta\theta \sim 6°$ to 10° and an in-plane texture $\Delta\phi \sim 6°$ to 15°, depending on the specific rolling and annealing conditions, as well as material purity, with a grain size ranging from ~30 to 100 μm in diameter. The 125-μm-thick Ni substrates were used as-rolled and annealed with no subsequent polishing. We grew the epitaxial oxide buffer layers, along with the *c*-axis–oriented, in-plane–aligned YBCO films, by pulsed-laser deposition (PLD), using a KrF excimer laser.

Typically, the epitaxial growth of a (001)-oriented cubic oxide on a Ni (001) surface is inhibited by the formation of NiO (111) at the oxide-metal interface (*22*). The Ni substrates were annealed at 900°C in a mixture of 4% H_2 and 96% Ar gas before film growth to reduce any NiO on the substrate surface. In order to further suppress the formation of NiO and achieve (001)-oriented epitaxy directly on the Ni (001) surface, we introduced H_2 gas into the PLD chamber during the initial stages of CeO_2 growth. Hydrogen is effective in reducing NiO while having little effect on the CeO_2 film. This (001)-oriented CeO_2 layer provides an oxide template directly on the metal surface for the subsequent epi-

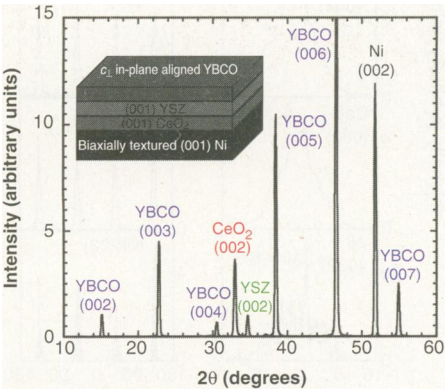

Fig. 1. An XRD θ-2θ scan, along with a schematic representation, of a YBCO/YSZ/CeO_2/Ni multilayer structure. The XRD scan shows the out-of-plane (001) orientations of the YBCO and oxide buffer layers.

taxial growth of additional oxide buffer and HTS layers. An alternative approach has also been developed that utilizes Pd as an epitaxial noble-metal interface between the oxide buffer layers and Ni substrate to inhibit the formation of NiO (*21*).

After the CeO_2 film was deposited, we grew a YSZ layer in situ, using PLD. The YSZ layer appears to alleviate cracking of the oxide layers that can occur due to the thermal expansion mismatch between the Ni substrate and the oxides. The CeO_2 and YSZ layers are each ~500 nm thick. A thick (>0.5 μm) YBCO film was then deposited at 780°C in an O_2 pressure of 185 mtorr. After deposition, the films were cooled at 10°C per minute, with the O_2 pressure increased to 700 torr at 400°C.

A θ-2θ x-ray diffraction (XRD) scan of a YBCO/YSZ/CeO_2 composite structure (Fig. 1) reveals that the CeO_2 and YSZ buffer layers, as well as the YBCO layer, are (001)-oriented relative to the surface normal. The intensity ratio of the CeO_2 (111)/(200) peaks is $<10^{-2}$, indicating a very small volume percentage of (111)-oriented oxide. The out-of-plane crystallographic texture for the YBCO, YSZ, CeO_2, and Ni can be determined by XRD rocking curves (θ scans) (Fig. 2). The rocking curve through the Ni (002) peak shows a significant amount of structure, due to the coarse-grained nature of the rolled-textured substrate, yielding an out-of-plane FWHM of ~6°. Subsequent rocking curves through the (002) peaks for the CeO_2 and YSZ layers indicate an out-of-plane FWHM of 5.5° and 5°, respectively. Some structure was also observed in these rocking curves, reflecting the good epitaxial relation between the oxides and the underlying Ni grains. A significant narrowing in the out-of-plane texture was observed for the YBCO, with the rocking curve through the YBCO (005) peak yielding an out-of-plane FWHM of only 1°. This improvement in the out-of-plane alignment relative to the underlying Ni results from the low (001) surface energy and the anisotropic film growth nature commonly observed for YBCO (6). This high degree of out-of-plane texture is important in realizing a high J_c, as it virtually eliminates the [100] tilt boundary contribution to the total misorientation angle of the grain boundaries.

The in-plane crystallographic alignment of the epitaxial YBCO/YSZ/CeO_2/Ni structure, as determined by XRD ϕ scans through the YBCO (226), YSZ (202), CeO_2 (202), and Ni (222), is also shown in Fig. 2. The in-plane FWHM for all of the layers is ~6.8°, indicating excellent epitaxy of the oxide layers with the biaxially textured metal. If the grain-to-grain misorientation angles are uncorrelated with a normal distribution, ~90% of the Ni grains have in-plane misorientation angles of 7° or less (*23*). The in-plane CeO_2 (100) and YSZ principal crystallographic axes are rotated 45° relative to the in-plane Ni (100) axis, whereas the *a* and *b* axes of the YBCO are rotated 45° with respect to the YSZ axes, all of which are in agreement with near-coincidence site lattice models (*24*). According to the high-resolution XRD scans, the lattice parameters for the YBCO film are very similar to those reported for fully oxygenated bulk materials, with $a = 3.82$ Å, $b = 3.88$ Å, and $c = 11.691$ Å. The normally cubic CeO_2 and YSZ layers show a slight tetragonal distortion, with the in-plane $a = b = 5.41$ Å, out-of-plane $c = 5.422$ Å for the CeO_2, and $a = b = 5.12$ Å, $c = 5.162$ Å for the YSZ layer. The tetragonal distortion of the oxide buffer layers appears related to the larger thermal expansion coefficient of the Ni substrate relative to these oxides, which tends to place the oxides in compression upon cooling after film growth.

The resistivity, ρ, and J_c values for various samples were measured with a standard four-point contact technique. The superconducting transition temperature, T_c (zero resistance), for the YBCO films was typically ~88 K. In the *a*–*b* plane at 300 K, ρ is ~250 μohm-cm with a linear resistivity that extrapolates to zero near 0 K, which is consistent with a high-quality, in-plane–aligned YBCO film with little grain-boundary scattering in the normal state. The magnetic field dependence of J_c at 77 K for a 1.4-μm-thick YBCO film deposited on a RABiTS tape is shown in Fig. 3 with magnetic field, *H*, applied parallel and perpendicular to the *c* axis.

Using a voltage criterion of 1 μV/cm, we measured the J_c of the ~3-mm-wide sample on a bridge that was 200 μm wide and 3 mm long patterned by standard photolithography. (Similar results have been obtained on 1-mm-wide bridges.) At zero field, this YBCO film has a J_c(77 K, $H = 0$) of 575,000 A/cm^2. We have produced several films with J_c(77 K, $H = 0$) greater than 600,000 A/cm^2; the highest value obtained thus far was 700,000 A/cm^2. These zero–magnetic field values are comparable to those obtained by using IBAD (*15*–*19*) and are within a factor of 4 of those observed for epitaxial YBCO films grown on polished $SrTiO_3$ (001). The magnetic field dependence of J_c for the film on rolled-textured Ni is similar to that measured for the epitaxial YBCO film on $SrTiO_3$. In fact, the relative drop of J_c with applied external magnetic field is less for the YBCO film grown on the Ni tape than for the film on $SrTiO_3$ (001), indicating the presence of additional flux-pinning defects

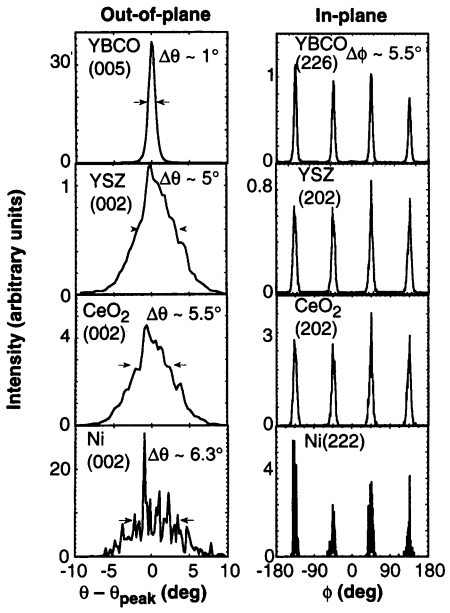

Fig. 2. XRD rocking curves and ϕ scans showing the out-of-plane and in-plane texture of a YBCO/YSZ/CeO_2 multilayer structure on a rolled-textured Ni substrate.

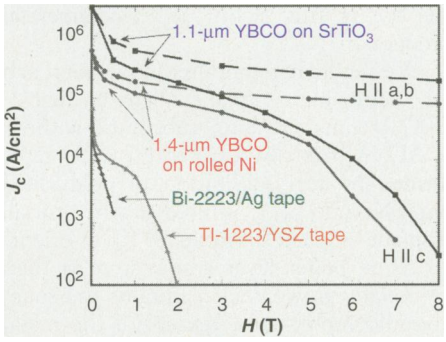

Fig. 3. Magnetic field dependence of J_c, measured at 77 K, for a YBCO/YSZ/CeO_2/rolled-textured Ni (001) structure. Also shown is $J_c(H, 77\ K)$ for YBCO on $SrTiO_3$ (001), Tl-1223 on polycrystalline YSZ (*27*), and Bi-2223/Ag tape (*26*).

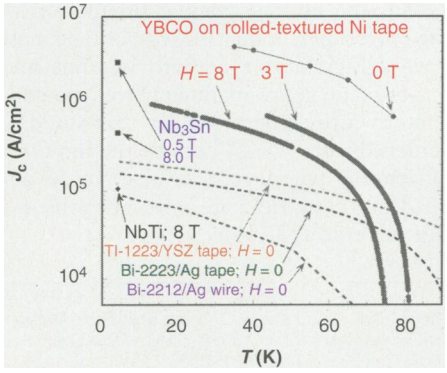

Fig. 4. The temperature dependence of J_c, measured at 0, 3, and 8 T, for a YBCO/YSZ/CeO_2/rolled Ni structure. For comparison, data are also shown for Bi-2212/Ag wire, (*29*), Bi-2223/Ag tape (*30*), Tl-1223/YSZ (*27*), NbTi (*28*), and Nb_3Sn (*28*).

in the films grown on the rolled-textured Ni. These pinning sites may be associated with growth-induced defect structures (*25*) or low-angle grain boundary pinning, or both (*16*, *17*). The $J_c(77\ K, H)$ behavior for $Bi_2Sr_2Ca_2Cu_3O_y$ (Bi-2223)/Ag (*26*) and $TlBa_2Ca_2Cu_3O_{8+x}$ (Tl-1223)/YSZ (*27*) tapes are also shown for comparison.

The temperature (T) dependence of J_c, measured in magnetic fields of 0, 3, and 8 T applied parallel to the YBCO c axis, is shown in Fig. 4. The $J_c(T)$ behavior for the YBCO films on the rolled-textured Ni tapes is comparable with that observed for epitaxial films on oxide single crystals, which is consistent with the absence of high-angle grain boundaries in the YBCO film. For comparison, we also show data for conventional low-T_c superconducting NbTi and Nb_3Sn wires (T_c is the superconducting transition temperature) (*28*) as well for $Bi_2Sr_2CaCu_2O_x$ (Bi-2212)/Ag (*29*), Bi-2223/Ag (*30*), and Tl-1223/poly-YSZ (*27*) HTS wires and tapes. Clearly, the performance of the epitaxial YBCO on rolled-textured Ni tape, in terms of J_c, is far superior to that of these other superconducting wire technologies, both for zero–magnetic field and high–magnetic field applications. In particular, the zero-field J_c of the YBCO on rolled Ni at 77 K is significantly higher than the J_c of state-of-the-art Bi-2223, Bi-2212, or Tl-1223 wires and tapes at 4.2 K. In addition, $J_c(T, H = 8\ T)$ for the YBCO/RABiTS is higher than $J_c(T, H = 0)$ for the Bi-2223/Ag and Tl-1223/YSZ wires in zero field at all $T < 65$ K. At $T < 40$ K, $J_c(H)$ for these films is greater than for conventional low-T_c superconductors, such as NbTi and Nb_3Sn, operating at 4.2 K. Thus, the use of rolling textured metal substrates, coupled with the epitaxial growth of appropriate buffer layer architectures and superconducting films, represents a viable means for producing long superconducting tapes for high-current, high-field applications at 77 K, particularly if high values of the "engineering" J_c, defined as the critical current per total conductor cross-sectional area (including substrate thickness), can be realized with thinner substrates or thicker YBCO films.

REFERENCES AND NOTES

1. J. W. Ekin, K. Salama, V. Selvamanickam, *Nature* **350**, 26 (1991).
2. D. T. Shaw, *Mater. Res. Soc. Bull.* **17**, 39 (1992); E. E. Hellstrom, *ibid.*, p. 45.
3. J. M. Phillips, *J. Appl. Phys.* **79**, 1829 (1996).
4. D. Dimos, P. Chaudhari, J. Mannhart, F. K. LeGroves, *Phys. Rev. Lett.* **61**, 1653 (1988).
5. D. Dimos, P. Chaudhari, J. Mannhart, *Phys. Rev. B* **41**, 4038 (1990).
6. D. P. Norton *et al.*, *Appl. Phys. Lett.* **57**, 1164 (1990).
7. Z. G. Ivanov *et al.*, *ibid.* **59**, 3030 (1991).
8. R. Gross and B. Mayer, *Physica C* **180**, 235 (1991).
9. M. F. Chisholm and S. J. Pennycook, *Nature* **351**, 47 (1991).
10. M. Kawasaki *et al.*, *Appl. Phys. Lett.* **62**, 417 (1993).
11. E. Sarnelli, P. Chaudhari, W. Y. Lee, E. Esposito, *ibid.* **65**, 362 (1994).
12. S. E. Babcock, X. Y. Cai, D. C. Larbalestier, D. L. Kaiser, *Nature* **347**, 167 (1990).
13. D. K. Christen *et al.*, in *Superconductivity and Its Applications*, H. S. Kwok, D. T. Shaw, M. J. Naughton, Eds. (American Institute of Physics, New York, 1993), vol. 273, p. 24.
14. M. Rupp, A. Gupta, C. C. Tsuei, *Appl. Phys. Lett.* **67**, 291 (1995).
15. Y. Iijima, N. Tanabe, O. Kohno, Y. Ikeno, *ibid.* **60**, 769 (1992).
16. R. P. Reade, P. Berdahl, R. E. Russo, S. M. Garrison, *ibid.* **61**, 2231 (1992).
17. X. D. Wu *et al.*, *ibid.* **67**, 2397 (1995).
18. M. Fukutomi, S. Aoki, K. Komori, R. Chatterjee, H. Maeda, *Physica C* **219**, 333 (1994).
19. F. Yang, E. Narumi, S. Patel, D. T. Shaw, *ibid.* **244**, 299 (1995).
20. H. Makita, S. Hanada, O. Izumi, *Acta Metall.* **36**, 403 (1988).
21. A. Goyal *et al.*, *Appl. Phys. Lett.* **69**, 1795 (1996).
22. N. N. Khoi, W. W. Smeltzer, J. D. Embury, *J. Electrochem. Soc.* **122**, 1495 (1975).
23. E. D. Specht *et al.*, *Physica C* **226**, 76 (1994).
24. J. D. Budai, R. T. Young, B. S. Chao, *Appl. Phys. Lett.* **62**, 1836 (1993).
25. D. H. Lowndes *et al.*, *Phys. Rev. Lett.* **74**, 2355 (1995).
26. S. Kobayashi, T. Kaneko, T. Kato, J. Fujikami, K. Sato, *Physica C* **258**, 336 (1996).
27. J. E. Tkaczyk *et al.*, *Appl. Phys. Lett.* **62**, 3031 (1993).
28. D. R. Tilley and J. Tilley, *Superfluidity and Superconductivity* (IOP Publishing, Bristol, UK, ed. 3, 1990), p. 235.
29. R. Wesche, *Physica C* **246**, 186 (1995).
30. P. Haldar, J. G. Hoehn Jr., J. A. Rice, M. S. Walker, L. R. Motowidlo, *Appl. Phys. Lett.* **61**, 604 (1992).

31. This research was sponsored by ORNL, managed by Lockheed Martin Energy Research Corporation, for the U.S. Department of Energy Office of Energy Efficiency and Renewable Energy and Office of Energy Research, under contract DE-AC05-96OR22464.

1 July 1996; accepted 30 August 1996

Creation of Nanocrystals Through a Solid-Solid Phase Transition Induced by an STM Tip

Jian Zhang,* Jie Liu,* Jin Lin Huang, Philip Kim, Charles M. Lieber†

A scanning tunneling microscope (STM) was used to fabricate T-phase tantalum diselenide ($TaSe_2$) nanocrystals with sizes ranging from 7 to more than 100 nanometers within the surface layer of 2H-$TaSe_2$ crystals at liquid helium temperature. Atomic-resolution images elucidate the structural changes between T- and H-phase regions and were used to develop an atomic model that describes a pathway for the production of T-phase nanocrystals from the H-phase crystal precursor through a solid-solid phase transition. The size-dependent properties of these nanocrystals may lead to improved understanding of the physics of charge density waves in small structures.

The development of new methods for the preparation of nanostructures is important in both meso- and nanoscale research because it is often the creation of these structures that limits studies of potentially interesting physical phenomena. Scanned probe microscopes, such as STMs and atomic force microscopes (AFMs), can in principle both create and probe the properties of very small nanoscale structures. For example, the STM has been used to manipulate individual atoms and molecules into structures (*1*–*4*), to probe quantum behavior in several nanostructures (*5*, *6*), and to lithographically pattern surfaces (*7*, *8*). The AFM has also been used to create nanostructures, including electronic (*9*) and mechanical (*10*) devices, by selective oxidation and nanomachining.

J. Zhang, J. Liu, J. L. Huang, Department of Chemistry, Harvard University, Cambridge, MA 02138, USA.
P. Kim and C. M. Lieber, Department of Chemistry and Division of Applied Sciences, Harvard University, Cambridge, MA 02138, USA.

*These authors contributed equally to this work.
†To whom correspondence should be addressed.

We report here an approach for the fabrication of nanostructures that uses the tip of an STM to drive a solid-solid phase transition in which 2H-$TaSe_2$ is transformed locally to nanometer-scale domains of T-phase $TaSe_2$. Both 1T- and 2H-$TaSe_2$ are layered materials consisting of covalently bonded two-dimensional (2D) Se–Ta–Se layers in which the Se atom sheets exhibit a hexagonal close-packed structure and the Ta atoms are in octahedral (1T) or trigonal prismatic (2H) holes defined by the two Se sheets. The 3D structure of these materials consists of stacks of the three-atom layers, ... Se–Ta–Se/Se–Ta–Se ..., that are held together by weak dispersion forces (*11*, *12*). The structural parameters of 2H-$TaSe_2$ (a = 3.43 Å; $c/2$ = 6.35 Å) and 1T-$TaSe_2$ (a = 3.48 Å; c = 6.26 Å) are similar. The electronic properties of these two phases, which are defined primarily by trigonal prismatic or octahedral bonding in a single layer, are quite distinct: 2H-$TaSe_2$ exhibits a weak charge density wave (CDW) that forms at 122 K and becomes